

Measurement of Glucose in Water with First-Overtone Near-Infrared Spectra

KEVIN H. HAZEN,* MARK A. ARNOLD,† and GARY W. SMALL

Department of Chemistry and Optical Science and Technology Center, University of Iowa, Iowa City, Iowa 52242 (K.H.H., M.A.A.); and Center for Intelligent Chemical Instrumentation and Department of Chemistry, Ohio University, Athens, Ohio 45701 (G.W.S.)

Partial least-squares (PLS) regression analysis was used to build calibration models for three unique spectral data sets of glucose in water. Spectra in the first data set were collected with a 2.0 mm optical pathlength. For these data, the measured root-mean-square (rms) noise of 100% lines over the 5975–5850 cm^{-1} spectral range was 4.5 micro-absorbance units (μAU). Spectrometer upgrades permitted a 5.2 mm optical pathlength for the second data set, and the resulting spectra had an rms noise of 5.9 μAU . Further spectrometer adjustments allowed the use of a 10.0 mm optical pathlength for the third data set, and the resulting spectral rms noise was 8.4 μAU . In each case, the instrumentation was modified individually in order to provide high radiant powers at the detector while avoiding detector saturation. Poor calibration models for the first data set indicate that a 2.0 mm optical pathlength is insufficient for adequate glucose measurements at clinically relevant concentrations. Calibration and prediction errors for the data collected at 5.2 and 10.0 mm pathlengths ranged from 0.40–0.50 and 0.35–0.40 mM, respectively. Digital Fourier filtering significantly improved model performance by reducing the required number of latent variables (factors) in the PLS models and by reducing the wavelength dependency of these models. For the best calibration model, spectra in the data set corresponding to a 10.0 mm pathlength were Fourier filtered with a Gaussian-shaped filter defined in digital frequency units (f) by a mean position of 0.0206 f and a standard deviation width of 0.0031 f . These filtered spectra were then submitted to a one-factor PLS model that is limited to the 5975–5850 cm^{-1} spectral range. Consideration of different spectral ranges and an analysis of spectral loading vectors indicate that the 5920 cm^{-1} absorption band for glucose is critical for useful analytical measurements.

Index Headings: Near-infrared spectroscopy; Spectroscopic glucose measurements; Partial least-squares regression; Digital Fourier filtering.

INTRODUCTION

In pursuit of the direct noninvasive measurement of glucose in human tissue, several studies have illustrated the determination of clinically relevant levels of glucose in biological samples from near-infrared (near-IR) spectra collected over the combination band region (4800–4200 cm^{-1}).^{1–11} Unfortunately, the transmission of light at these wavelengths is poor through human tissue. Scattering processes and strong absorption by water and fatty tissue¹² severely reduce the optical throughput in this region. When a solid-state near-IR detector is used in conjunction with a blackbody source and Fourier transform spectrometer, the intrinsic detector noise is often the limiting noise source of the measurement. In this case, reduced optical throughput causes a significant increase in

spectral noise and renders this spectral region unacceptable for noninvasive measurements. For this reason, the first-overtone region (6500–5500 cm^{-1}) and shorter wavelengths have been proposed for noninvasive blood glucose measurements.^{12–24} Absorption properties of human tissue are less severe in the first-overtone region; however, scattering effects are more pronounced.

The poor transmission properties of human tissue in the combination band region motivate an evaluation of the first-overtone region for measuring glucose at physiological levels in aqueous media. This report details our ability to measure clinically relevant levels of glucose from first-overtone near-IR spectra. The effects of optical pathlength and spectral range are established for a series of multivariate calibration models computed through the application of partial least-squares (PLS) regression to both raw and digitally filtered spectra. The relationship between spectral quality and model performance is also evaluated for spectra collected from three different spectrometer configurations.

EXPERIMENTAL

Apparatus and Reagents. Spectra were collected with a Nicolet 740 Fourier transform spectrometer (Nicolet Analytical Instruments, Madison, WI) equipped for the near-IR region by use of a calcium fluoride beam-splitter and a 2 mm² cryogenically cooled indium antimonide (InSb) detector. Incident light was restricted to the range of 6579–5540 cm^{-1} (1.52–1.81 μm) by use of a standard H-band interference filter (Barr Associates, Westford, MA). This filter transmitted 78% of the incident light at 5920 cm^{-1} . Different source powers, aperture settings, and software gain settings were used for samples with different optical pathlengths. For the 2 mm samples, the standard 75 W tungsten-halogen lamp was replaced with a 150 W lamp. The aperture and gain settings were 125 and 1, respectively. These settings are specified in the arbitrary units selected in the Nicolet SX software that controlled the spectrometer. A setting of 330 corresponds to the widest aperture. A 250 W lamp was used for the 5.2 and 10 mm samples, with the aperture and gain set at 70 and 4, respectively, for the 5.2 mm samples, and 330 and 4, respectively, for the 10 mm samples.

Samples were contained in a temperature-controlled cell mount (Wilmad, Buena, NJ) equipped with two sapphire windows (25 mm diameter and 0.9 mm thick). Temperatures were maintained at 37.0 (± 0.1) °C with a VWR Model 1140 refrigerated water bath (VWR Scientific, Chicago, IL). Temperatures were monitored by placing a copper-constantan thermocouple (Omega, Inc., Stamford, CT) directly in the sample solution within the sample

Received 29 May 1998; accepted 24 August 1998.

* Present address: Instrumentation Metrics, Inc., 2085 Technology Circle, Suite 201, Tempe, AZ 85284.

† Author to whom correspondence should be sent.

TABLE I. Specifications for glucose data sets.

	2.0 mm pathlength	5.2 mm pathlength	10.0 mm pathlength
Number of samples	67	63	73
Number of spectra	200	185	219
Mean glucose conc. (mM)	12.73	13.69	13.15
Standard deviation of glucose conc. (mM)	7.25	7.63	7.69
Glucose conc. range (mM)	1.35–24.9	2.13–28.6	1.19–28.1

holder. An Omega 670 digital meter was used to read solution temperatures.

All glucose solutions were prepared by dissolving dried reagent-grade glucose in a pH 7.4 working buffer. This buffer was composed of 0.1 M phosphate and 0.483 g/L 5-fluorouracil (preservative). Buffer solutions were prepared with type I reagent-grade water obtained from a three-stage Milli-Q water purification unit (Millipore, Inc., Bedford, MA). Actual glucose concentrations were determined by using a YSI 2300 STAT Plus analyzer (Yellow Springs Instruments, Inc., Yellow Springs, OH).

Procedures. Double-sided interferograms consisting of 16 384 points were collected on the basis of 256 coadded scans. These interferograms were triangularly apodized and Fourier transformed to produce single-beam spectra with a point spacing of 1.9 cm^{-1} . This high level of resolution was used to remain consistent with our earlier work in the combination region. Mertz phase correction was applied with a phase array based on 200 points on each side of the interferogram center burst. The resulting single-beam spectra were transferred to a Silicon Graphics Indigo workstation (Silicon Graphics, Mountain View, CA) for further processing. The spectral processing software used on the Silicon Graphics system was implemented in FORTRAN 77. Subroutines used in implementing the digital filtering and multiple linear regression calculations were taken from the IMSL software package (IMSL, Inc., Houston, TX).

For each pathlength, spectra were collected during a single data collection session. Spectra were collected in a random order with respect to glucose concentration. All spectra were collected in triplicate without removing the sample from the spectrometer. Three background spectra of glucose-free buffer were collected after every third sample. Table I summarizes the number of samples and the corresponding number of spectra for each data set. One spectrum in the 2 mm data set and four spectra in the 5.2 mm data set were inadvertently lost while being transferred to the Indigo workstation. Table I also provides the mean, standard deviation, and range of glucose concentrations in each of these data sets. For the 2.0 mm data set, all spectra corresponding to 10 and 9 randomly selected samples were placed in the monitoring and prediction data sets, respectively. For the 5.2 mm data, all spectra for nine randomly selected samples were placed in the monitoring data set and a second group of spectra corresponding to another set of nine samples was placed in the prediction data set. For the 10.0 mm data, the monitoring and prediction data sets corresponded to all spectra associated with two unique groups of 10 randomly selected samples.

Calibration models were developed with spectra in ab-

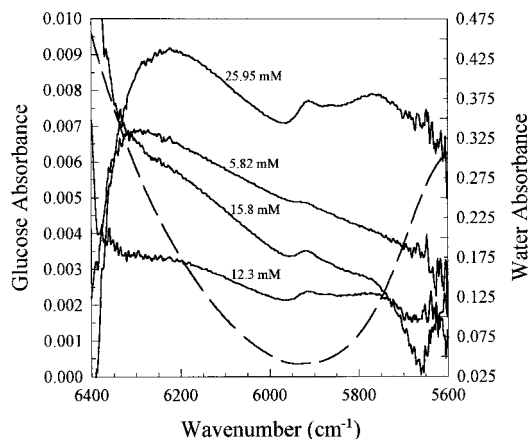


FIG. 1. Absorbance spectra for water (broken line) and glucose solutions (solid lines) with the indicated concentrations.

sorbance units by use of the same procedures described in previous work.^{4,7,9} The spectra in absorbance units were computed by dividing each single-beam spectrum by the immediately preceding background spectrum and then converting the resulting transmittance values to absorbance. When necessary, Fourier filtering was implemented by subjecting the entire spectrum (full spectral range) to the digital Fourier filter algorithm and then selecting the required spectral range for analysis. A random number generator was used to distribute the samples into separate calibration, monitoring, and prediction data sets. All spectra for a given sample were moved as a group, and no sample was used in more than one data set. All spectra corresponding to nine or ten samples were placed in the monitoring and prediction data sets.

RESULTS AND DISCUSSION

Absorption Bands and Spectral Range. The relative position and size of the absorption bands for water and glucose are presented in Fig. 1. This water absorbance spectrum corresponds to a spectrum of a 1 mm thick sample of the working buffer referenced to an air background spectrum. Although the presented spectral range corresponds to a window between two water absorption bands centered at 6870 and 5200 cm^{-1} , the magnitude of the water absorbance is considerably greater than that for glucose. The glucose absorbance spectra were computed by use of a background spectrum of the working buffer and are presented for a series of glucose standards with an optical pathlength of 10 mm. These spectra reveal absorption features centered at 6200 , 5920 , and 5775 cm^{-1} . The relatively strong absorbance from water overshadows the broad and poorly distinguished bands centered at 6200 and 5775 cm^{-1} . These findings corroborate earlier work to identify glucose in concentrated dry mixtures and fruit juice samples.^{25,26}

An important parameter used in computing a multivariate calibration model is the spectral range supplied to the model building method. When latent variable methods such as PLS regression are employed to build calibration models, the spectral range dictates which spectral points are used in the computation of the latent variables. The spectral range should include information describing the concentration variation of the analyte and other ma-

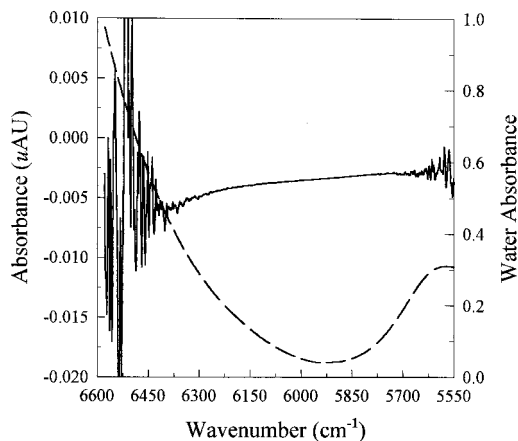


FIG. 2. Representative 100% line for overtone spectra (solid line) computed from two water spectra collected sequentially. A water absorbance spectrum (broken line) is superimposed for comparison. The pathlength for the 100% line spectra was 10 mm and the pathlength for the water absorbance spectrum was 1 mm.

trix constituents while excluding regions dominated by noise or other artifacts that might become incorporated into the model on the basis of chance correlations. Suitable spectral ranges can be identified by either a statistically driven optimization scheme, such as a modified grid search or a genetic algorithm,^{27–32} or an arbitrary selection on the basis of known absorption properties for the analyte of interest. The second method was used here, given the simplicity of the sample matrix and the well-defined spectral features for glucose.

The following spectral ranges were examined for the glucose models: 6579–5540, 6300–5700, 6300–5975, 5975–5850, and 5850–5700 cm^{-1} . This first range corresponds to the 50% transmission frequencies of the incident radiation and, therefore, essentially represents the whole spectral range. The second range includes all three glucose absorption bands but trims the high noise and limited glucose information at the higher and lower frequency extremes. The last three ranges isolate each of the three glucose absorption features (see Fig. 1).

Spectral quality ultimately limits the analytical utility of absorption spectroscopy since the spectral signal-to-noise ratio (SNR) dictates the limit of detection. Spectral quality can be conveniently presented as the root-mean-square (rms) noise on 100% lines. In this work rms noise levels were measured for 20 different buffer spectra collected with each spectrometer configuration. The 100% lines were generated by dividing the second and third

replicate spectra for each sample and converting to absorbance units. Ideally, replicate spectra are identical, which would create 100% lines that are horizontal and flat at zero absorbance.

A typical 100% line is presented in Fig. 2 along with an absorbance spectrum of water. For near-IR spectra through aqueous samples, the SNR is not constant across the spectrum, but depends on the frequency of the radiation. This frequency dependency is illustrated in Fig. 2, where considerably greater noise is evident at both the high and low frequency extremes (i.e., greater than 6375 cm^{-1} and less than 5700 cm^{-1}). The absorption characteristics of water are responsible for the frequency dependency. A water absorbance spectrum is superimposed on the 100% line in Fig. 2 to show how the spectral noise correlates with water absorption. Under our spectrometer conditions, the spectral measurements are detector-noise limited, which means the noise is constant across the spectrum. The SNR of the measurement, however, depends on the optical throughput.³³ Higher radiant powers at the detector produce larger signals, thereby providing greater SNRs and superior spectral quality. Conversely, limited optical throughput results in low radiant powers, poor SNRs, and higher spectral noise. Of course, the optical throughput is lower at radiant frequencies strongly absorbed by water and, as a result, the SNR is poor at these frequencies. Finally, computed rms noise on 100% lines depends on the specific spectral region selected.

Actual 100% lines are not typically horizontal but appear slightly curved. This curvature is caused by slight differences in the spectral collection conditions between replicates. This difference is frequency dependent and typically corresponds to slight differences in sample temperature. In addition, 100% lines can be offset from zero because of frequency-independent differences in data collection parameters. A difference in instrument alignment between replicates is a possible example.

Root-mean-square noise levels can be computed about a quadratic least-squares regression curve for a defined region of the 100% line. The second-order fit accounts for the curvature within this spectral region, thereby providing a better estimate of spectral noise. Table II lists normalized noise values computed by dividing the mean rms noise computed across the 20 buffer samples by the sample thickness ($\mu\text{AU}/\text{mm}$). These noise values are normalized in this manner simply to facilitate direct comparison between instrument configurations. For each data set, the spectral noise is lowest for the 5975–5850 cm^{-1}

TABLE II. Noise and PLS model parameters for the three spectral data sets.

Range ^a	2.0 mm pathlength				5.2 mm pathlength				10.0 mm pathlength			
	N/b ^b	Fact ^c	SEC ^d	SEP ^e	N/b ^b	Fact ^c	SEC ^d	SEP ^e	N/b ^b	Fact ^c	SEC ^d	SEP ^e
6579–5540	120	21	1.49	2.60	265	21	0.92	1.56	316	12	3.13	4.00
6300–5700	27.3	13	1.28	1.02	3.21	12	0.32	0.72	5.00	18	0.13	0.44
6300–5975	8.65	9	5.21	4.66	2.27	11	1.46	2.44	3.49	9	2.95	3.58
5975–5850	2.25	7	1.81	1.68	1.18	7	0.55	0.55	0.84	4	0.43	0.42
5850–5700	2.71	7	5.85	5.77	2.08	5	3.29	2.66	2.97	11	2.88	3.71

^a Spectra range (cm^{-1}).

^b Average rms noise computed across 100% lines divided by sample thickness ($\mu\text{AU}/\text{mm}$).

^c Optimum number of PLS factors.

^d Standard error of calibration (mM).

^e Standard error of prediction (mM).

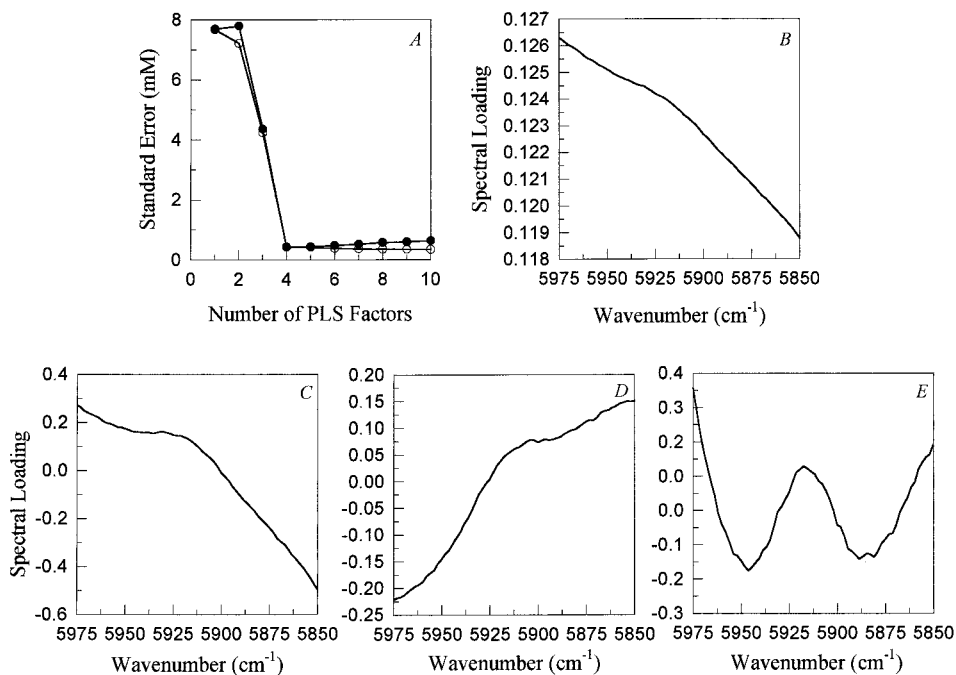


FIG. 3. Plot of standard errors of calibration and prediction vs. the number of PLS factors (A) and spectral loading plots for the first (B), second (C), third (D), and fourth (E) PLS factors for the 5975–5850 cm^{-1} PLS model.

spectral range, which corresponds to the region with greatest optical throughput (lowest water absorbance, see Fig. 2). Noise levels are larger for all other spectral ranges as the optical throughput drops because of water absorption of light. It is difficult to compare noise levels across data sets. Such a comparison is complicated because different spectrometer configurations were used for each data set in order to minimize noise in the 5975–5850 cm^{-1} region. In addition, transmission spectra of water are not linearly related to optical pathlength, which results in nonlinear dependencies in spectral quality. Experimentally, the lowest overall normalized noise corresponds to the 10 mm pathlength data with the 5975–5850 cm^{-1} spectral range. For all other spectral ranges, the lowest normalized noises correspond to the 5.2 mm data set.

Partial Least-Squares Calibration Models. A series of PLS calibration models were computed for each data set by stepping the number of PLS factors from 1 to 30 for each of the five spectral ranges. The optimal number of PLS factors was determined as that which produced a minimum standard error of prediction (SEP). Performance parameters for the best calibration models are tabulated in Table II.

Within each data set, the best analytical performance comes from models restricted to the 5975–5850 cm^{-1} spectral range. This range encompasses the 5920 cm^{-1} glucose band and possesses the lowest spectral noise. Similar performance is noted for the 6300–5700 cm^{-1} spectral range, which incorporates both the 5920 and 5775 cm^{-1} glucose bands. In fact, the lowest prediction errors for the 2.0 mm data set come from this wider spectral range. It must be noted, however, that the 6300–5700 cm^{-1} model requires nearly double the number of latent variables to achieve this performance. In fact, all models computed over the 6300–5700 cm^{-1} spectral range re-

quire more latent variables relative to the corresponding 5975–5850 cm^{-1} models. More complex models are necessary to accommodate greater spectral variation and higher spectral noise in this wider range.

Poor models result from the remaining three spectral regions where noise levels are too high to allow glucose information to be extracted reliably. Although the widest spectral range (6579–5540 cm^{-1} incorporates all three glucose absorption bands, the large noise levels at both the high and low frequency extremes greatly degrade the ability to retrieve this glucose information. Similarly, the relatively high noise levels of the other restricted spectral regions (6300–5975 and 5850–5700 cm^{-1}) coupled with the poor quality of the corresponding glucose absorption bands severely limits calibration performance.

Comparison across data sets reveals that models corresponding to the 5.2 and 10.0 mm data sets significantly outperform models from the 2.0 mm data set. In fact, prediction errors are unacceptably high for all calibration models generated with the data collected with a 2.0 mm pathlength. Even though the overall spectral noise is below 5 μAU across the 5975–5850 cm^{-1} spectral region, prediction errors are greater than 1.6 mM when the sample thickness is only 2.0 mm. In this case, even with a low noise level, there is simply not sufficient glucose absorbance to allow a viable calibration model to be constructed. Longer pathlengths and lower noise result in superior model predictions for the 5.2 and 10.0 mm data sets.

The best calibration model uses only four factors to provide a measurement error of 0.4 mM. This model corresponds to the 5975–5850 cm^{-1} spectral range with a 10.0 mm optical pathlength. A plot of measurement error as a function of model size (for the first 10 factors) is provided in Fig. 3 along with a series of plots showing the spectral loadings for each factor of the optimum four-

factor model. The large errors noted in Fig. 3A for the first model factor indicate that this factor incorporates little glucose-specific information. Inspection of the spectral loading plot for this first factor (Fig. 3B) confirms the lack of glucose information in the factor. Lower measurement errors are obtained with the second, third, and fourth factors, which suggest the presence of glucose-specific information in these factors. Indeed, spectral loading plots for these latent variables (Figs. 3C, 3D, and 3E) reveal significant contributions of the spectral information corresponding to the glucose band centered at 5920 cm^{-1} . In fact, the magnitude of the glucose band appears largest for the fourth factor, and this factor provides the greatest drop in measurement error. This strong correlation between the model performance and the appearance of glucose spectral features within individual model factors is direct evidence that the PLS algorithm is modeling glucose.

Similar glucose absorption features are evident in spectral loading plots for the other spectral ranges. Generally, glucose features are most evident in loadings associated with large decreases in measurement error. The ability to distinguish analyte spectral features in these loading plots diminishes as the spectral noise increases and other nonanalyte-dependent spectral variations dominate the spectra.

Fourier Filtering. Digital Fourier filtering is an effective preprocessing tool for enhancing spectral signal-to-noise by reducing both high- and low-frequency noise within near-IR spectra.^{4,7-10} This preprocessing method is particularly effective at reducing the impact of baseline variations, such as those induced by temperature differences between the sample and background spectra.⁷ For this reason, we have evaluated Fourier filtering as a means to enhance the PLS calibration models for glucose computed from overtone spectra.

As in previous work, a Gaussian-shaped frequency response function was used to filter the Fourier transformed spectra.^{4,7-10} The position and width of this filter correspond to the mean and standard deviation of the Gaussian function positioned along a digital frequency (f) axis that linearly spans values from 0 to $0.5 f$. As detailed before, a grid search method was used here to identify the optimum combination of mean position and standard deviation width.^{4,7-9} In this work, spectra collected with a given optical pathlength were separated into three data sets. For comparison purposes, the calibration and prediction data sets were identical to those used above for processing raw spectra. The remaining spectra were placed into a monitoring data set that was used to establish the optimum combination of position and width for the filter frequency response function.

Optimum filter parameters were established by assessing all combinations of 80 possible mean positions and 50 possible standard deviation widths. Tested mean values ranged from 0 to $0.048 f$ with $0.0006 f$ step sizes and tested standard deviations ranged from 0 to $0.025 f$ with $0.0005 f$ step sizes. For each combination of mean and standard deviation, PLS models were generated with the correspondingly Fourier filtered spectra in the calibration data set. For each combination of mean and standard deviation, PLS models were constructed with 1 to 20 factors. Once computed, each model was used to pre-

dict the glucose concentrations corresponding to the spectra in the monitoring set. Model performance was assessed by computing an objective function defined as the reciprocal of the sum of mean squared errors of the calibration and monitoring data ($1/[\text{MSEC} + \text{MSEM}]$, where MSEC and MSEM correspond to the mean-squared errors computed with the calibration and monitoring spectra, respectively). Three-dimensional surface plots of the objective function vs. the filter position and width were constructed to identify the optimum filter parameters (lowest combination of calibration and monitoring errors). PLS calibration models with 1 to 30 factors were then generated with spectra treated by the optimized Fourier filter, and the ideal number of model factors corresponded to that which gave the lowest SEP. This optimization procedure was repeated for each spectral range and optical pathlength.

Several trends became apparent while generating the 400 surface plots described above. Typical surface plots are presented in Fig. 4 that correspond to the 10 mm data set over the $5975\text{--}5850\text{ cm}^{-1}$ spectral range. For these data, the use of a single PLS factor during filter optimization provides a well-defined peak (see Fig. 4A). For a given standard deviation, the response value increases and then decreases as the mean position of the frequency response function is scanned across this peak. With three PLS factors, a ridge begins to form where the peak mean position increases as the standard deviation increases (see Fig. 4B). In fact, the peak mean value for a given standard deviation is roughly twice that of the standard deviation. Because 95% of the area of the Gaussian frequency response function lies within two standard deviations of the mean, such a ridge structure indicates that very low digital frequencies (i.e., baseline deviations) are being rejected for all filters defined by values riding along the top of this ridge. By the time five PLS factors are involved, many combinations of mean and standard deviation provide roughly equivalent calibration and monitoring errors (see Fig. 4C). Recalling that four PLS factors are optimal when processing these raw, unfiltered spectra, the surface plot in Fig. 4C indicates that model performance is relatively insensitive to Fourier filtering, because this number of PLS factors can essentially model any unfiltered spectral features (i.e., baseline variations). The use of more than five factors results in large, noisy, poorly defined surface plots characteristic of over-modeling.

Surface plots for other spectral ranges are similar to those described above. Generally, a sharp peak is found with few factors, a ridge forms with an intermediate number of factors, and a noisy plateau forms when the number of factors used in the optimization matches the optimum number found with raw unfiltered spectra. In general, more factors are needed to achieve optimal performance as the spectral range is widened and more noise is incorporated into these models. For the $5975\text{--}5850$, $6579\text{--}5540$, and $6300\text{--}5700\text{ cm}^{-1}$ spectral ranges, 5, 13, and 19 factors are required to produce the noisy plateau structures typified in Fig. 4C.

Optimum values for the mean position and standard deviation width are similar for all five spectral ranges. These values are summarized in Table III for the 10.0 mm pathlength data. In addition, these values are similar

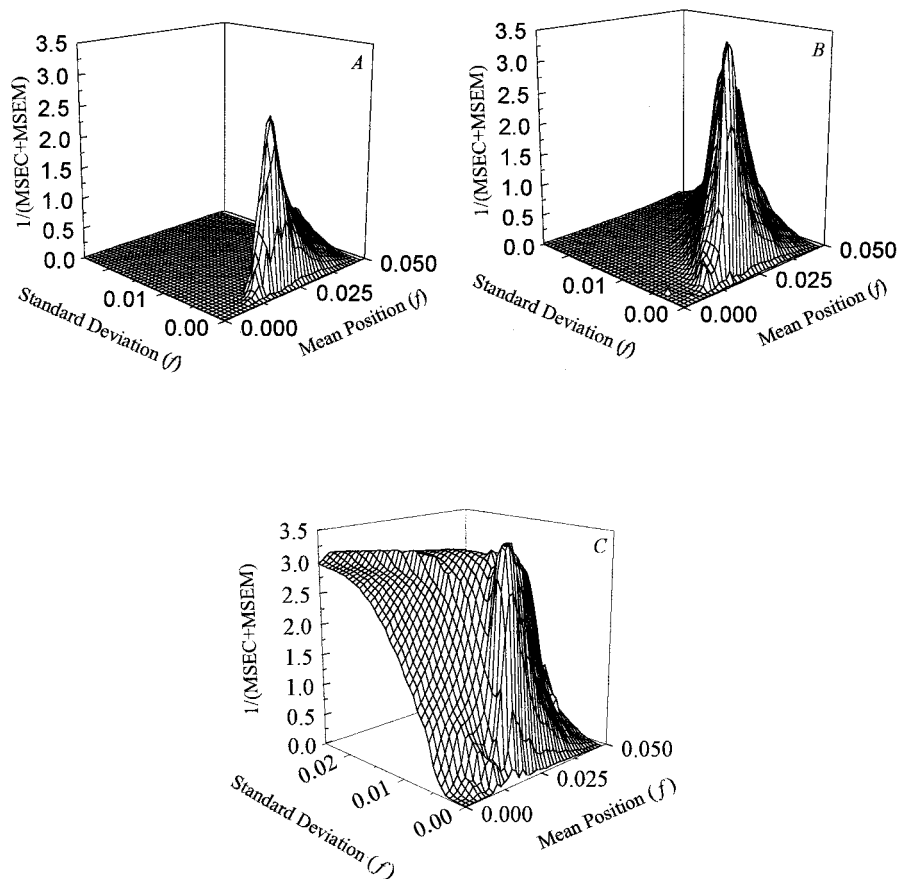


FIG. 4. Surface plots for optimizing Fourier filter parameters for the 5975–5850 cm^{-1} spectral region when using one (A), three (B), and five (C) PLS factors.

to those found optimal for reducing noise and baseline variations in near-IR spectra collected over the combination band region (4800–4200 cm^{-1}).^{1,4–10} As noted before, this type of Fourier filtering is relatively insensitive to the shape of these near-IR absorption bands for specific chemical species.⁴

PLS calibration models from Fourier filtered spectra were computed for each optical pathlength and each spectral range. In all cases, the optimum Fourier filter parameters were used, and the number of model factors was stepped from 1 to 30. Results from PLS models providing the lowest SEP for each optical pathlength are tabulated in Table IV.

The effectiveness of Fourier filtering as a preprocessing step is demonstrated by comparing performance from PLS models built with filtered and unfiltered spectra. Comparison of results in Tables II and Table IV reveals that calibration and prediction errors are generally lower and/or fewer factors are typically required for models

from filtered spectra. Furthermore, calibration and prediction errors are consistent for all spectral ranges for both the 5.2 and 10.0 mm pathlength data sets. Consistency across spectral ranges is not observed with the unfiltered data. The Fourier filtering step reduces spectral noise across the entire spectrum, thereby rendering the analysis less sensitive to spectral range. In general, measurement errors are approximately 1–2 mM for the 2 mm pathlength data, 0.4–0.5 mM for the 5.2 mm pathlength data, and 0.35–0.40 mM for the 10.0 mm pathlength data.

The effectiveness of Fourier filtering is further evident by comparing spectra before and after being passed through this digital filter. The spectra presented in Fig. 5A correspond to a representative series of raw absorbance spectra in the 10 mm data set. Although the glucose features can be distinguished in some of these spectra, baseline curvature and offsets make visual quantification difficult. The spectra in Fig. 5B are obtained after passing the raw absorbance spectra through a Fourier filter. For this filter, the mean position and standard deviation width are 0.0206 and 0.0031 f , respectively, which match the optimal values found for the 5975–5850 cm^{-1} spectral region. The impact of Fourier filtering is striking, with a clearly distinguishable feature corresponding to the 5920 cm^{-1} glucose absorption band. As Fourier filtered spectra resemble derivative spectra, the zero crossings at 5885 and 5940 cm^{-1} represent inflection points along the glucose absorption band, and the minima at 5865 and 5965 cm^{-1} correspond to the base of this glu-

TABLE III. Optimum Gaussian filter parameters for the 10.0 mm data set.

Spectral range (cm^{-1})	Mean position (f)	Standard deviation width (f)
6579–5540	0.0204	0.0035
6300–5700	0.0258	0.0055
6300–5975	0.0198	0.0025
5975–5850	0.0206	0.0031
5850–5700	0.0186	0.0020

TABLE IV. PLS model parameters for Fourier filtered spectra.

Range ^a	2.0 mm pathlength			5.2 mm pathlength			10.0 mm pathlength		
	Fact ^b	SEC ^c	SEP ^d	Fact ^b	SEC ^c	SEP ^d	Fact ^b	SEC ^c	SEP ^d
6579–5540	23	1.23	1.03	11	0.53	0.41	14	0.38	0.39
6300–5700	21	1.47	0.81	11	0.40	0.41	9	0.35	0.34
6300–5975	18	1.37	1.55	14	0.55	0.44	10	0.35	0.38
5975–5850	11	2.06	1.69	6	0.55	0.52	1	0.46	0.40
5850–5700	7	2.37	1.96	5	0.77	0.56	10	0.40	0.40

^a Spectral range (cm⁻¹).

^b Optimum number of PLS factors.

^c Standard error of calibration (mM).

^d Standard error of prediction (mM).

cose band. These points are roughly identifiable in the unfiltered spectra shown in Fig. 5A.

In general, Fourier filtering improves model performance by enhancing the SNR values for these spectra. The improved performance is most striking for the 10.0 mm data set over the 5975–5850 cm⁻¹ spectral range. In this case, a single PLS factor is sufficient to measure clinically relevant levels of glucose. The concentration correlation plot for this model is presented in Fig. 6. Calibration, monitoring, and prediction data closely follow the ideal unity line. As expected for an SEP of 0.40, the scatter in this plot indicates a prediction capability of ± 1 mM.

As displayed by the solid line in Fig. 7, the first, and only, spectral loading vector for the model represented in Fig. 6 resembles the spectral features of Fourier filtered

glucose spectra. Fourier filtered spectra are also plotted in Fig. 7 over the 5975–5850 cm⁻¹ spectral range. The mean and standard deviation for this filter are the optimal values for the model (i.e., 0.026 and 0.0031 f , respectively). Filtered spectra are presented for a series of samples with glucose concentrations ranging from 4.43 to 28.1 mM. Clearly, this spectral loading vector is essentially identical to the filtered glucose absorption feature in this spectral range.

CONCLUSION

PLS analysis of raw overtone spectra indicates that the 5920 cm⁻¹ glucose band is critical for useful calibration models. Glucose bands centered at 6200 and 5775 cm⁻¹ do not provide sufficient information owing to high spectral noise in these regions. As expected for information derived from absorbance spectra, longer optical pathlengths and lower spectral noise yield superior prediction errors for spectral regions that encompass the 5920 cm⁻¹ glucose band.

Direct comparison between the different data sets is complicated by the fact that both pathlength and spectral noise vary between these data sets. Ideally, one would

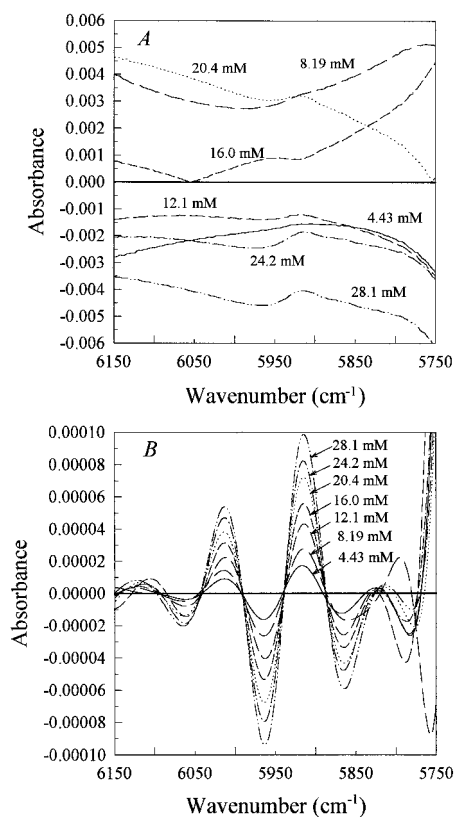


FIG. 5. Raw (A) and Fourier filtered (B) overtone spectra for a series of samples with the indicated glucose concentrations. The Fourier filter used a mean position of 0.0206 f and standard deviation width of 0.0031 f for the Gaussian frequency response function.

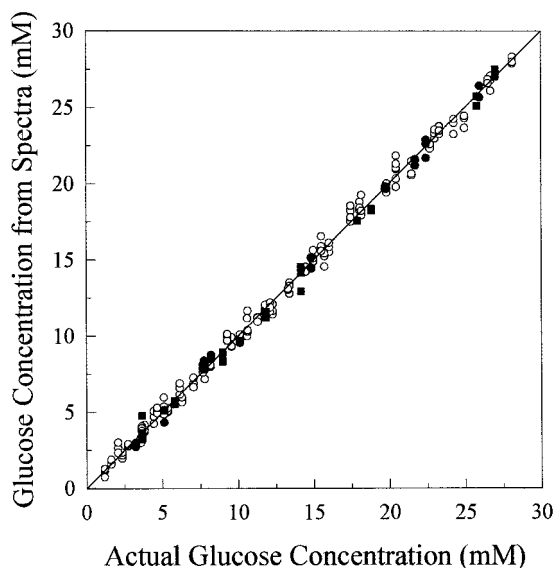


FIG. 6. Concentration correlation plot for the 5975–5850 cm⁻¹ model with one PLS factor and a Fourier filter with a frequency response function specified by a mean position of 0.0206 f and standard deviation width of 0.0031 f . Symbols indicate calibration (○), monitoring (■), and prediction (●) spectra.

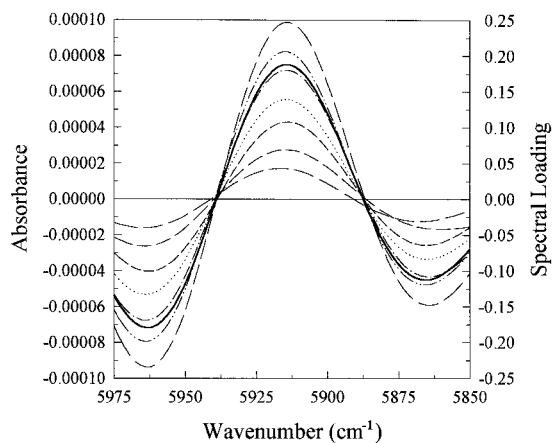


FIG. 7. Spectral loading vector (solid line) for the calibration model defined in Fig. 6 superimposed on Fourier filtered glucose absorbance spectra over the 5975–5850 cm^{-1} spectral range. Glucose concentrations from bottom to top at 5920 cm^{-1} are 4.43, 8.19, 12.1, 16.0, 20.4, 24.2, and 28.1 mM.

like to keep the normalized noise ($\mu\text{AU}/\text{mm}$) constant across the data sets in order to assess pathlength effects. Nevertheless, useful information can be extracted from these data in terms of the pathlength. For example, we can say that a 2 mm optical pathlength is insufficient for sound glucose measurements when the spectral noise is 2.25 $\mu\text{AU}/\text{mm}$ or greater. Even with digital filtering to enhance signal-to-noise, prediction errors range from 1 to 2 mM for the 2 mm pathlength data. Acceptable calibration models can be achieved by increasing the optical pathlength to 5.2 mm with a concomitant decrease in spectral noise (1.18 $\mu\text{AU}/\text{mm}$). Measurement errors drop to ~ 0.4 –0.5 mM. By increasing the optical pathlength to 10.0 mm and lowering the spectral noise to 0.84 $\mu\text{AU}/\text{mm}$, the best analytical performance is achieved with the fewest model factors. In this case, prediction errors are 0.35–0.4 mM.

These findings demonstrate the critical relationship between optical pathlength, spectral noise, and measurement error. This relationship has important implications for the potential of measuring blood glucose noninvasively from overtone spectra. Successful noninvasive blood glucose measurements require long optical pathlengths through the medium of interest combined with low spectral noise. It would not be possible to measure millimolar levels of glucose with overtone spectra when the optical pathlength is less than 2 mm unless the spectral noise is significantly less than 2.25 $\mu\text{AU}/\text{mm}$. An approach based on diffuse reflectance measurements would be challenging given the limited effective optical pathlengths that are possible owing to small penetration depths of radiation at these wavelengths into skin tissue.³⁴ Clearly, pathlength and spectral noise must be considered when designing a noninvasive blood glucose system, and these parameters must be reported when describing such instrumentation.

It is also important to stress that the findings reported here were obtained under the simplest possible matrix conditions with glucose dissolved in temperature-controlled, nonscattering aqueous solutions. For this reason, the prediction errors reported here are certainly overly

optimistic as an indicator of analytical performance for noninvasive blood glucose measurements. Although our analysis of the spectral loading vectors clearly indicate the existence of glucose-specific information in the PLS calibration models, the existence of information related to the displacement of water by glucose cannot be ignored. The extent to which water displacement information is incorporated into these models will over estimate prediction abilities because such information will not be available from spectra collected in more complex, multi-component systems such as spectra collected noninvasively from human subjects. Finally, the complexities associated with scattering, temperature, pressure, and chemical interferences will further degrade performance when the system is extended to noninvasive human measurements.

ACKNOWLEDGMENTS

We wish to acknowledge Ms. Mary Pollard for her contributions in the early phases of this project. The financial support from the National Institute of Diabetes and Digestive and Kidney Diseases (DK-45126) is greatly appreciated.

1. K. H. Hazen, M. A. Arnold, and G. W. Small, *Anal. Chim. Acta* **371**, 255 (1998).
2. J. J. Burmeister, M. A. Arnold, and G. W. Small, *IEEE Lasers and Electro-Optics Society* **12**, (1998).
3. M. J. Mattu, G. W. Small, and M. A. Arnold, *Anal. Chem.* **69**, 4696 (1997).
4. S. Pan, H. Chung, M. A. Arnold, and G. W. Small, *Anal. Chem.* **68**, 1124 (1996).
5. M. A. Arnold, *Current Opinion in Biotech.* **7**, 46 (1996).
6. M. A. Arnold, in *Handbook of Clinical Laboratory Automation, Robotics, and Optimization*, G. J. Kost, Ed. (John Wiley and Sons, New York, 1996), Chap. 26, pp. 631–647.
7. K. H. Hazen, M. A. Arnold, and G. W. Small, *Appl. Spectrosc.* **48**, 477 (1994).
8. L. A. Marquardt, M. A. Arnold, and G. W. Small, *Anal. Chem.* **65**, 3271 (1993).
9. G. W. Small, L. A. Marquardt, and M. A. Arnold, *Anal. Chem.* **65**, 3279 (1993).
10. M. A. Arnold and G. W. Small, *Anal. Chem.* **62**, 1457 (1990).
11. J. W. Hall and A. Pollard, *Clin. Biochem.* **26**, 483 (1993).
12. J. J. Burmeister, M. A. Arnold, and G. W. Small, *Photochemistry and Photobiology (Symposium-in-print)* **67**, 50 (1998).
13. H. M. Heise, in *Biosensors in the Body*, D. M. Fraser, Ed. (John Wiley and Sons, New York, 1997), Chap. 3, pp. 79–116.
14. H. M. Heise, *Horm. Metab. Res.* **28**, 527 (1996).
15. H. M. Heise, R. Marbach, Th. Koschinsky, and F. A. Gries, *Artif. Organs* **18**, 439 (1994).
16. H. M. Heise and R. Marbach, *Proc. SPIE* **2089**, 114 (1994).
17. R. Marbach, Th. Koschinsky, F. A. Gries, and H. M. Heise, *Appl. Spectrosc.* **47**, 875 (1993).
18. H. M. Heise and R. Marbach, *Proc. SPIE* **1575**, 507 (1991).
19. J. Qu and B. C. Wilson, *J. Biomed. Optics* **2**, 319 (1997).
20. M. Kohl, M. Essenpreis, and M. Cope, *Phys. Med. Biol.* **40**, 1267 (1995).
21. U. A. Muller, B. Mertes, C. Fischbacher, K.-U. Jagemann, and K. Danzer, *Int. J. Artif. Organs* **20**, 285 (1997).
22. C. Fischbacher, K.-U. Jagemann, K. Danzer, U. A. Muller, L. Papenkordt, and J. Schuler, *Fresenius' J. Anal. Chem.* **359**, 78 (1997).
23. K.-U. Jagemann, C. Fischbacher, K. Danzer, U. A. Muller, and B. Mertes, *Z. Phys. Chem.* **191**, 179 (1995).
24. M. R. Robinson, R. P. Eaton, D. M. Haaland, G. W. Hoeppe, E. V. Thomas, B. R. Stallard, and P. L. Robinson, *Clin. Chem.* **38**, 1618 (1992).
25. R. Giangiacomo, J. B. Magee, G. S. Birth, and G. G. Dull, *J. Food. Sci.* **46**, 531 (1981).
26. R. Giangiacomo and G. G. Dull, *J. Food. Sci.* **51**, 679 (1986).
27. M. J. McShane, G. L. Coté, and C. H. Spiegelman, *Appl. Spectrosc.* **52**, 878 (1998).

28. C. H. Spiegelman, M. J. McShane, M. J. Goetz, M. Motamedi, Q. L. Yue, and G. L. Côté, *Anal. Chem.* **70**, 35 (1998).
29. A. S. Bangalore, R. E. Shaffer, G. W. Small, and M. A. Arnold, *Anal. Chem.* **68**, 4200 (1996).
30. R. E. Shaffer, G. W. Small, and M. A. Arnold, *Anal. Chem.* **68**, 2663 (1996).
31. J. M. Brenchley, U. Horchner, and J. H. Kalivas, *Appl. Spectrosc.* **51**, 689 (1997).
32. P. J. Brown, *J. Chemom.* **6**, 151 (1992).
33. P. R. Griffiths and J. A. de Haseth, *Fourier Transform Infrared Spectrometry*, (Wiley-Interscience, New York, 1986), Chap. 7.
34. R. Marbach and H. M. Heise, *Appl. Opt.* **34**, 610 (1995).